ADVANCED OPTICAL MATERIALS
www.advopticalmat.de

Hybrid Silicon All-Optical Switching Devices Integrated with 2D Material

Daiki Yamashita, Nan Fang, Shun Fujii, and Yuichiro K. Kato**

Hybrid all-optical switching devices that combine silicon nanocavities and 2D semiconductor materials are proposed and demonstrated. By exploiting the refractive index modulation caused by photo-induced carriers in the 2D material instead of the silicon substrate, the switching speed limitation imposed by the carrier lifetime of silicon is overcome while maintaining a low switching energy. Air-mode photonic crystal nanobeam cavities capable of efficient interaction with 2D materials are fabricated, and molybdenum ditelluride, a 2D material with rapid carrier recombination, is transferred onto the cavities. The molybdenum ditelluride flake is excited by an optical pump pulse to shift the resonant wavelength of the cavity for switching operation. All-optical switching operations are achieved on the time scale of tens of picoseconds while requiring low switching energies of a few hundred femtojoules.

1. Introduction

Silicon photonics has emerged as a compelling platform for the creation of photonic integrated circuits (PICs), enabling monolithic co-integration of electronic and photonic elements on a single semiconductor chip.[1–3] Within PICs, optical switching stands as an elemental and pivotal function, being responsible for routing and modulation of optical signals. While optical switches actuated by mechanical, electrical, and thermal means have been extensively studied,[4] the increasing need for faster speed and more energy-efficient operation has shifted the focus to all-optical switching.[5] In particular, index modulation through photo-induced carriers is a commonly used method for controlling optical signals by another incident beam of light.

For efficient photo-excitation, all-optical switches based on microcavities are advantageous as they enhance light-matter interactions by spatially confining light.[6–16] Although the use of microcavities has enabled ultrafast and energy-efficient switching, the performance is restricted by the intrinsic limitations of the silicon substrates.[7,8] To shorten the carrier lifetime of silicon for faster switching speed, ion implantation has been employed to achieve switching with a time scale of tens of picoseconds. Ion implantation, however, causes a large insertion loss for the signal light (>10 dB cm^{-1}),[6,9,11] which leads to inevitable performance deterioration in PICs. While different substrate materials such as organic composite materials,[10] III–V semiconductors,[6,12,13] and amorphous silicon[14] have been utilized for higher performance, the incompatibility to fabricate these materials directly on silicon substrates remains a critical barrier, challenging monolithic on-chip integration.

One promising avenue for mitigating this challenge lies in the use of hybrid systems that integrate disparate materials onto the silicon photonics platform.[17,18] Instead of direct growth, materials can be grown on separate substrates and then wafer bonded. Such hybrid systems have been effectively employed in a variety of PICs and have found utility in a range of optical devices, from lasers and modulators to photodetectors, primarily based on III–V semiconductors.[19,20]

As another candidate for this hybrid framework, 2D materials with unique optoelectronic properties have attracted considerable interest.[21–23] Remarkably, despite their atomically thin profiles, 2D layered materials exhibit pronounced light-matter interaction even for a monolayer.[24,25] Because of their diverse electronic configurations, these materials span an extraordinarily broad spectral range from ultraviolet to microwave frequencies.[26] In terms of the hybridization process, 2D materials can be grown directly on various substrates over large areas using chemical vapor deposition methods, making them

D. Yamashita, S. Fujii, Y. K. Kato
Quantum Optoelectronics Research Team
RIKEN Center for Advanced Photonics
Saitama 351-0198, Japan
E-mail: daiki.yamashita@aist.go.jp; yuichiro.kato@riken.jp
D. Yamashita
Platform Photonics Research Center
National Institute of Advanced Industrial Science and Technology (AIST)
Ibaraki 305-8568, Japan
N. Fang, Y. K. Kato
Nanoscale Quantum Photonics Laboratory
RIKEN Cluster for Pioneering Research
Saitama 351-0198, Japan
S. Fujii
Department of Physics
Faculty of Science and Technology
Keio University
Yokohama 223-8522, Japan

The ORCID identification number(s) for the author(s) of this article can be found under https://doi.org/10.1002/adom.202402531

DOI: 10.1002/adom.202402531

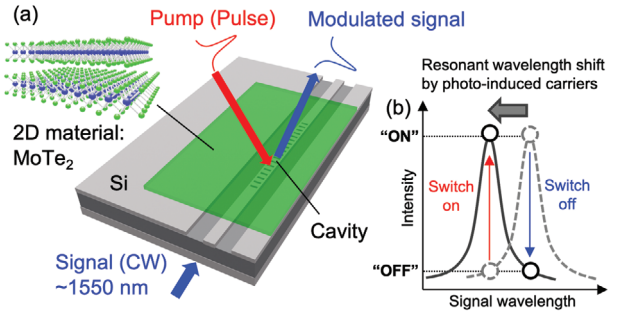

Figure 1. a) Schematic diagram of our proposed hybrid all-optical switching device in which a 2D material is loaded on top of a microcavity. b) Operating principle of all-optical switching using microcavities. Photo-induced carriers shift the resonant spectrum, enabling the selection of either switch-on or -off operation based on the signal wavelength.

compatible with complementary metal-oxide-semiconductor (CMOS) technologies.[27] In addition, the mechanical flexibility and van der Waals interfaces of 2D layered materials enable seamless integration into various photonic structures and the high uniformity at the atomic layer level ensures that light scattering loss is extremely small.[28] Owing to this optical versatility and inherent compatibility with the photonic structures, 2D material hybrids provide fruitful ground for the design and realization of next-generation all-optical switches; devices that require compact dimensions, high speed operation, superior efficiency, wide bandwidth, and cost effectiveness.

In this work, we demonstrate hybrid all-optical switching devices that combine silicon nanocavities and 2D semiconductor material. Refractive index modulation caused by photo-induced carriers in the 2D semiconductor allows us to achieve switching performance unconstrained by the properties of the silicon substrate. A thin 2D material flake characterized by rapid carrier recombination is integrated into a silicon nanocavity. The flake placed on top of the cavity is excited by an optical pump pulse, which induces a shift in the resonant wavelength of the cavity and thereby enabling the switching operation. We have successfully implemented high-speed all-optical switching with a shortened time scale of tens of picoseconds and low switching energy of a few hundred femtojoules.

2. Concept

Microcavity-based all-optical switching typically relies on changes in the refractive index of the substrate material, but we propose instead to use 2D semiconductor as the refractive index changing medium. **Figure 1**a shows a schematic of the all-optical switching device using a hybrid of a silicon microcavity and a 2D material. A thin 2D semiconductor flake is loaded onto a microcavity and excited by a pump pulse to generate carriers. As shown in Figure 1b, the refractive index modulation by the photo-induced carriers in the flake shifts the resonant wavelength of the cavity, thereby modulating the signal light input from the waveguide.

Based on this operating principle, we first design the cavity structure for fast and low-energy switching. It is necessary to reduce the device size for enhancing the interaction between light and the 2D semiconductor, and therefore we use a 1D photonic crystal (PhC) nanobeam cavity.[29,30] Compared to waveguide ring cavities, the PhC cavities have a larger mode overlap with low-dimensional materials.[31,32] To further enhance the interaction between light in the cavity and the 2D layered semiconductor, we employ air modes instead of the commonly used slab modes.[31–35] The air modes have a large mode overlap with the 2D material loaded on top of the cavity because the electric field is distributed in the air rather than in the dielectric material, and a slight modulation of the refractive index of the 2D layered semiconductor can efficiently shift the resonant wavelength.[32]

We now turn our attention to the 2D semiconductor used for refractive index modulation. For high-speed and low-energy operation, the material must be transparent in the telecom wavelength band, have large optical absorption for pump light, and have a short carrier lifetime. Molybdenum ditelluride ($MoTe_2$), which is one of the transition metal chalcogenide 2D semiconductors, meets the requirements. With a higher refractive index than silicon (Si), it allows for large modulation of the effective refractive index in the mode by photo-induced carriers. The carrier lifetime critical for the switching time can be as fast as a few picoseconds for excitons generated by optical absorption,[36] offering the potential for fast switching.

3. Results and Discussion

The hybrid switching device assembled from a PhC nanobeam cavity and a thin $MoTe_2$ flake is shown in **Figure 2**a. In implementing the cavity, we take into account the redshift after the integration of $MoTe_2$ to obtain the cavity resonant wavelength λ_{cav} near 1.55 µm. For low energy switching, a high-quality factor (Q) of the cavity ≈10 000 is desirable after transferring the 2D material. Resonant spectra are measured to investigate the change in the cavity resonant mode before and after the transfer of the $MoTe_2$ flake (Figure 2b). Although we observe a slight decrease in Q from 33 000 to 20 000 before and after the transfer, the Q remains sufficiently high for low-energy switching. It also suggests that the absorption of signal light by $MoTe_2$ and additional scattering introduced by the integration are small, allowing for low insertion loss operation.

Next, we characterize the optical properties of the transferred 2D flake to identify the bandgap and to determine the carrier lifetime. Figure 2c shows the photoluminescence (PL) spectrum of the flake, showing that $MoTe_2$ with a thickness of ≈10 nm is an indirect transition semiconductor with a band gap at ≈1.3 µm and the PL intensity is weak and negligible at λ_{cav}. The carriers dynamics is investigated by measuring the PL decay curves of the $MoTe_2$ flake on the cavity (Figure 2d). As $MoTe_2$ is known to degrade in air due to surface defect formation,[37] the same flake is measured on different days after the transfer. The surface defects in $MoTe_2$ increase the non-radiative rate, consequently reducing the PL lifetime.[36] The PL lifetime for either days (Day 1: 50 ps, Day 7: 19 ps) is much shorter than Si (≈ns in photonic crystals[9,38]), thus enabling fast switching with $MoTe_2$. It is interesting to note that the increased defect density is beneficial for our devices as it boosts the switching speed, whereas faster non-radiative rates generally imply performance degradation in light-emitting devices. The defect density in $MoTe_2$ progressively rises with air exposure, and encapsulating it with hexagonal boron nitride should prevent further introduction of defects for stabilizing the device performance at the optimum condition.[39]

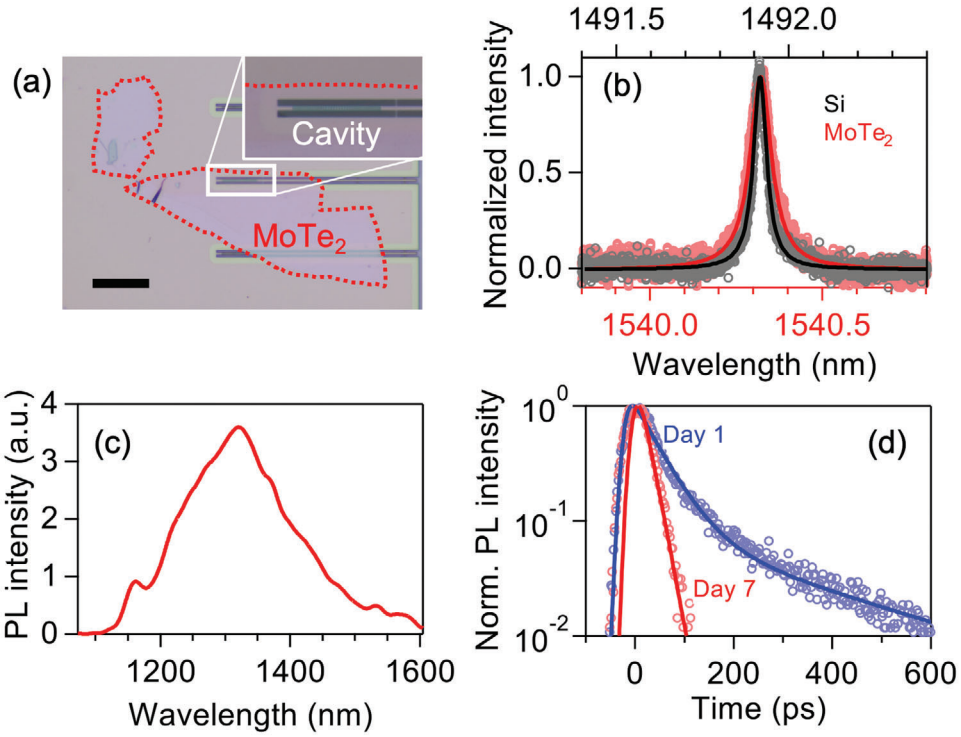

Figure 2. a) Optical micrograph of a hybrid Si cavity-based switching device integrated with an 11-nm-thick $MoTe_2$ flake. The scale bar is 20 μm. b) Resonant mode spectra before (black) and after (red) transfer of the $MoTe_2$ flake. The circles are data and the lines are Lorentzian fits. The resonant wavelength has shifted by 48.41 nm from 1491.91 to 1540.32 nm before and after the transfer, which is attributed to the increase in the effective refractive index of the cavity by $MoTe_2$.[32] c) PL spectrum of $MoTe_2$ on the switching device measured with continuous-wave excitation at 950 nm and 100 μW. (d) PL decay curves of $MoTe_2$ on the switching device obtained with 1000 nm and 256 fJ pulsed excitation for different dates. The circles are data, the line for Day 1 is a bi-exponential fit, and the line for Day 7 is an exponential fit. The τ_1 values for Day 1 and Day 7 are 50 and 19 ps, respectively. The τ_2 value for Day 1 is 309 ps.

We now examine the basic operation of the cavity-based all-optical switch. The $MoTe_2$ flake on the cavity is pumped by a pulsed laser to modulate the cavity mode. **Figure 3**a shows the time response of the signal light intensity with different signal laser wavelengths. It is noted that the switching response is normalized by dividing it with the intensity of the unmodulated signal light. Here, the signal wavelength detuning $\Delta\lambda_{sig}$ is defined as $\lambda_{sig} - \lambda_{cav}$, where λ_{sig} is the signal wavelength. For negative $\Delta\lambda_{sig}$, the switching response shows a rise in the normalized intensity and then a fallback to the baseline. At $\Delta\lambda_{sig} = -0.02$ nm, the peak intensity decreases and a dip appears. For positive $\Delta\lambda_{sig}$, the switching response exhibits a clear dip. These are typical switching characteristics of cavity-based all-optical switches as shown in Figure 1b, where operation is switch-on for negative detuning and switch-off for positive detuning. The detailed $\Delta\lambda_{sig}$ dependence is shown as a color plot in Figure 3b. Theoretical simulation of the switching response based on coupled mode theory[16,40,41] are consistent with experimental data (Section S1 and Figure S1a, Supporting Information).

In order to achieve a large modulation in switching, we explore the optimal signal wavelength that produces the maximum modulation. We define the modulation contrast as a difference between the maximum deviation at the peak or the dip and the baseline, and present the $\Delta\lambda_{sig}$ dependence of the modulation contrast in Figure 3c. Although symmetric amplitudes are expected for switch-on and switch-off operations, the resonant spectrum can become asymmetric due to free-carrier absorption (see Figure S1, Supporting Information).[42–45] The largest absolute value of the modulation contrast is obtained for a switch-off operation condition. In the following, experiments are performed with λ_{sig} which maximizes the absolute value of the modulation contrast.

For further increase of the switching performance, we look for the optimal pump wavelength recalling that the optical absorption and photo-induced carriers play a vital role in the switching dynamics. In **Figure 4**a, the switching response with different pump wavelength λ_{pump} is investigated. At shorter λ_{pump} (800, 850, and 900 nm), the modulation depth is approximately the same and the switching response has two components in the switching recovery time. As λ_{pump} increases (950 and 1000 nm), the slow component in the switching recovery time decreases and the modulation becomes larger, and then the modulation decreases at $\lambda_{pump} = 1050$ nm. The slow component shows larger absorption at shorter wavelengths, which can be attributed to the behavior of Si. The fast component is interpreted as absorption by $MoTe_2$, with a characteristic exciton resonance near 1000 nm.[46] The observed switching recovery times are consistent with carrier lifetimes in $MoTe_2$ and Si, respectively.[9,36,38]

To quantitatively investigate the contributions of the $MoTe_2$ and Si components to switching, we fit the switching recovery

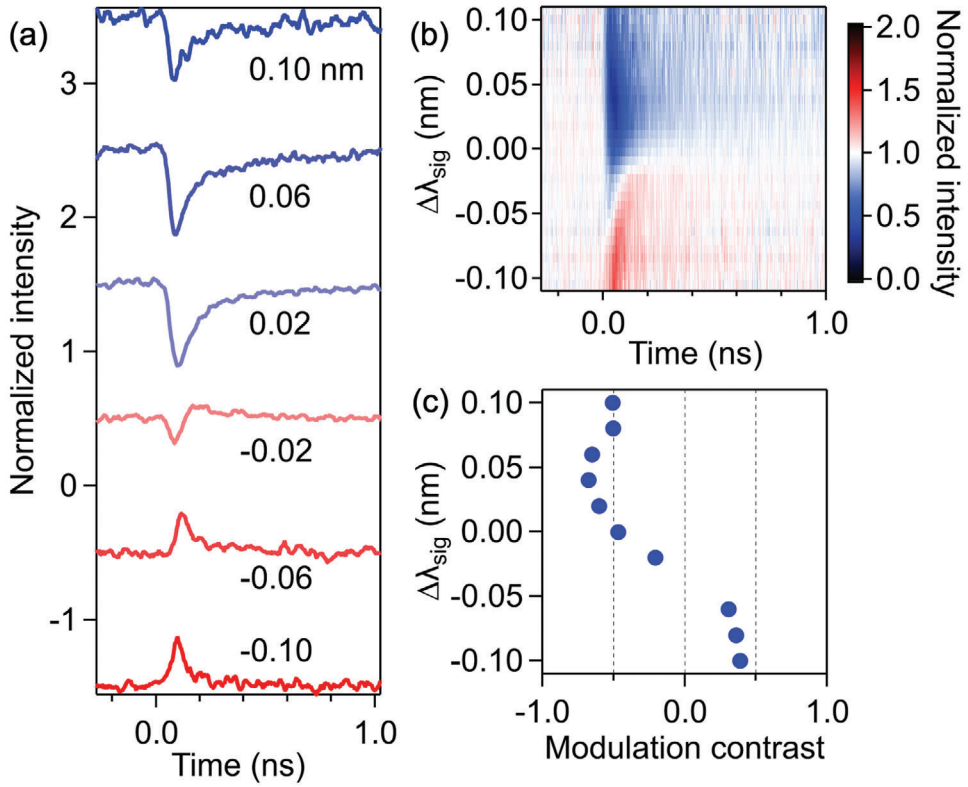

Figure 3. a) Switching response at different $\Delta\lambda_{sig}$. The response is normalized by the signal intensity in the absence of a pump laser. The pump wavelength and pump pulse energy are 950 nm and 256 fJ, respectively. The curves are offset for clarity. b) Color plot of the switching response at different $\Delta\lambda_{sig}$. The red color indicates peaks and the blue color indicates dips relative to the baseline of the signal intensity. c) Modulation contrast as a function of $\Delta\lambda_{sig}$.

curves. Assuming that the spectral shape of the resonant mode is Lorentzian and the shift in the resonant wavelength changes as a bi-exponential decay, the switching response can be described by[9]

$$I(t) = [\{a_1 e^{(-t/\tau_1)} + a_2 e^{(-t/\tau_2)}\}^2 + 1]^{-1} \quad (1)$$

where a_1 and a_2 are the amplitudes while τ_1 and τ_2 are the switching recovery times, with the subscripts 1 and 2 indicating the components for $MoTe_2$ and Si, respectively. We fit the curves in Figure 4a using $\tau_1 = 100$ ps and $\tau_2 = 3$ ns to obtain a_1 and a_2. In Figure 4b, we plot the λ_{pump} dependence of modulation depth caused by photo-induced carriers in $MoTe_2$ and Si. As λ_{pump} increases, the modulation originating from Si decreases due to a reduction in absorption. The modulation caused by $MoTe_2$ reaches its maximum value when λ_{pump} is ≈1000 nm, which is consistent with the λ_{pump} dependence of the PL intensity shown in Figure 4c, indicating that more photo-induced carriers lead to larger modulation. Consequently, to obtain large modulation and fast switching, the optimal λ_{pump} for this hybrid switch is ≈1000 nm where optical absorption is large and the slow switching component is small.

Finally, with the knowledge of the optimal signal and pump wavelengths, we evaluate the switching speed and energy of this $MoTe_2$ hybrid switch. For comparison, an all-silicon switching device with a similar Q of 26 000 is also examined. **Figure** 5a shows the switching response of the Si device and the $MoTe_2$ hybrid device, measured 2 and 6 days after sample fabrication. The fitting is performed using a single switching time component (τ_1) for Si and $MoTe_2$ Day 6 data and two switching time components (τ_1 and τ_2) for $MoTe_2$ Day 2 data. The τ_1 values for the Si, $MoTe_2$ Day 2, and Day 6 devices are 3600 ± 500 , 50 ± 10 , and 33 ± 5.5 ps, respectively. Remarkably, the switching speed of the Day 6 device is significantly faster—more than a hundredfold compared to the Si device. This acceleration is attributed to the rapid carrier recombination in $MoTe_2$, as shown in Figure 2d. The lack of the slow time component (τ_2) in the $MoTe_2$ Day 6 device is due to an increase in defects, leading to more absorption in $MoTe_2$ and thus less light reaching the Si substrate. The 33 ps switching speed is the fastest among PhC-cavity-based all-optical switches using Si as a substrate material.[8,9,15]

Defining the extinction ratio as the logarithm of the normalized signal intensity, Figure 5b–d displays the switching response of Si, $MoTe_2$ Day 2, and $MoTe_2$ Day 6 devices with different pump pulse energy U_{pump}. The $MoTe_2$ hybrid devices show larger modulation than the Si device, and the extinction contrast increases with increasing U_{pump} in all devices with no apparent saturation. Figure 5e summarizes the U_{pump} dependence of the extinction ratio value at the maximum deviation from the baseline for the three devices. The interpolated values of U_{pump} at 3 dB extinction contrast are 133 and 254 fJ for the Day 2 and Day 6 devices, respectively. These switching energies are more than

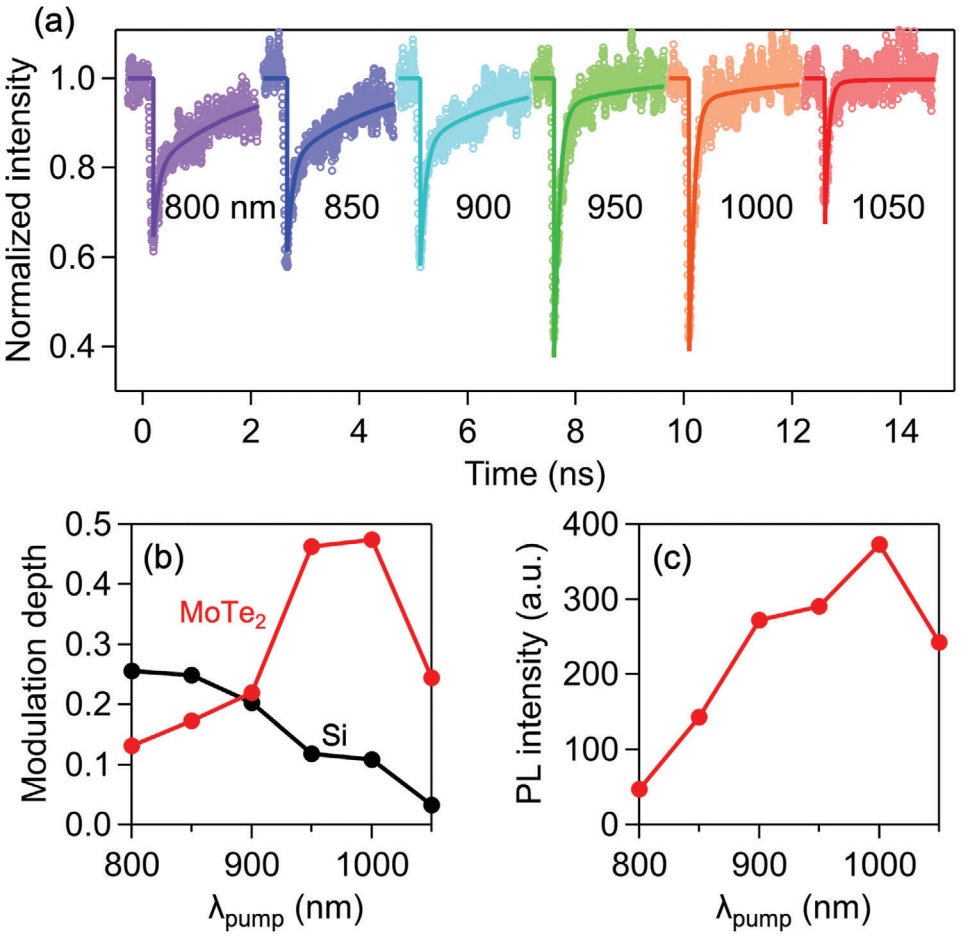

Figure 4. a) Switching response for different λ_{pump} with a pump pulse energy of 128 fJ. The circles are data and the lines are fits using Equation 1. b) λ_{pump} dependence of modulation depth caused by the photo-induced carriers in $MoTe_2$ (red) and Si (black). c) λ_{pump} dependence of the PL intensity from the $MoTe_2$ on the cavity measured by a superconducting single-photon detector.

one order of magnitude smaller than that of switching using Si ring cavities[7,11] and are comparable to switching using Si PhC cavities.[8,9,16]

4. Conclusion

In conclusion, we have developed a hybrid switching device that combines a PhC nanobeam cavity and a $MoTe_2$ flake to achieve high speed and low energy all-optical operation. Despite a slight decrease in cavity Q after $MoTe_2$ integration, the cavity maintains a high Q essential for low energy switching. $MoTe_2$ shows faster carrier recombination compared to Si, which enables increased switching speed. We have investigated the signal and pump wavelength dependence to maximize the modulation contrast and to improve the switching performance. Remarkably, the $MoTe_2$ hybrid device exhibits a switching time of 33 ps with a switching energy of a few hundred femtojoules, successfully overcoming the intrinsic switching speed limitation of Si while maintaining low switching energy.

To further increase the switching performance, confining the pump pulse light to the cavity resonant mode can make the switching energy low.[7–9,13,14] For the $MoTe_2$ flakes, fine tuning the surface defect density and thickness can improve the switching speed and switching energy. In addition, all-optical switching operation at different pump wavelengths is possible by changing the 2D material. Our proposed structure is compatible with CMOS technologies, thus demonstrating the potential for high-speed and low-energy operation in integrated all-optical switching systems.

5. Experimental Section

Sample Preparation: Air-mode nanobeam cavities, with an 800 nm width and a lattice constant of a = 350 nm,[32,35] feature a parabolically modulated lattice over 16 periods to create a central minimum optical potential. The cavities have air holes of $0.35a \times 500$ nm, and the cavity center has a period of $1.18a$. The nanobeam cavities were fabricated using silicon-on-insulator wafers with a top Si thickness of 260 nm and a buried oxide thickness of 1 µm. The nanobeams were patterned by electron beam lithography, followed by inductively-coupled plasma etching of the top Si layer. The buried oxide layer under the nanobeam structures was then etched with hydrofluoric acid. $MoTe_2$ crystals were purchased from HQ Graphene. $MoTe_2$ flakes were prepared on

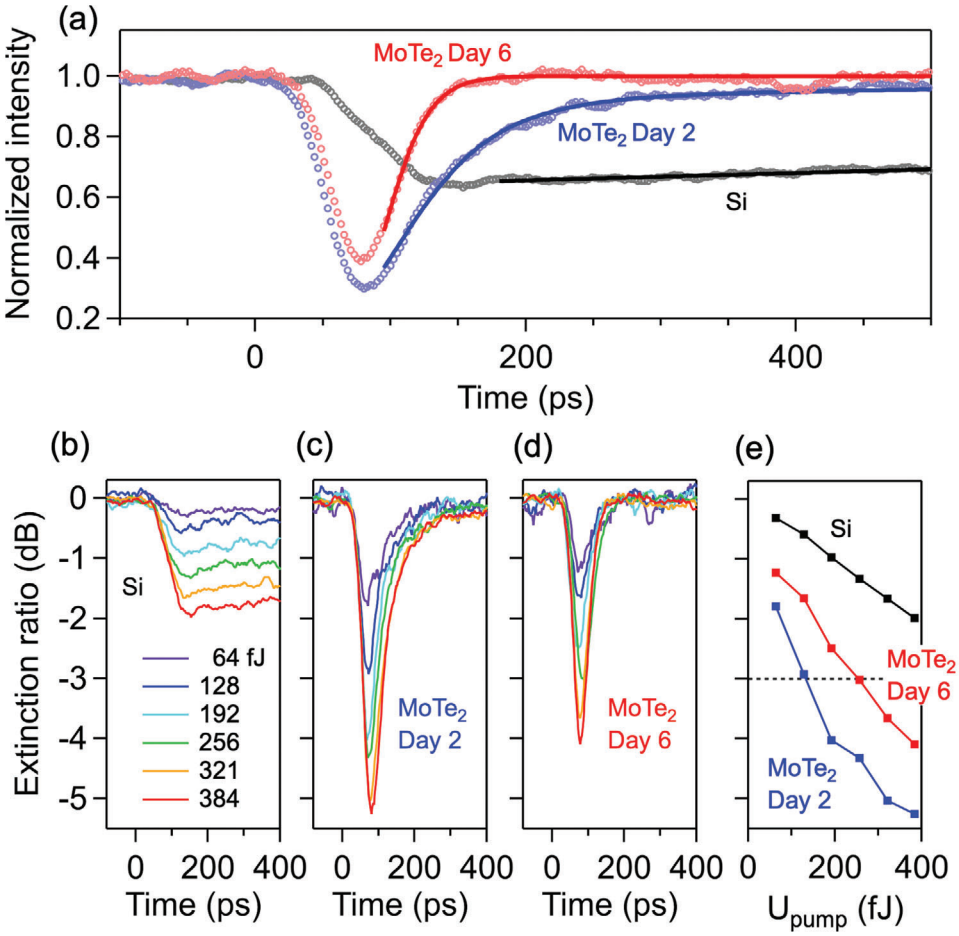

Figure 5. a) Switching response of the Si device (black), and the $MoTe_2$ device at 2 (blue) and 6 (red) days after sample fabrication. $\lambda_{pump} = 1,000$ nm and $U_{pump} = 384$ fJ. The circles are data, and the lines are fits using Equation 1. For the $MoTe_2$ Day 2 device, $\tau_1 = 50 \pm 10$ ps, $\tau_2 = 1,400 \pm 800$ ps, $a_1 = 0.78$, and $a_2 = 0.22$. Switching response of b) Si, c) $MoTe_2$ Day 2, and d) $MoTe_2$ Day 6 devices at different U_{pump}. e) U_{pump} dependence of extinction ratio for Si, $MoTe_2$ Day 2, and $MoTe_2$ Day 6 devices.

polydimethylsiloxane (PDMS) by employing a mechanical exfoliation technique. The $MoTe_2$ flakes are transferred onto the cavities using a conventional PDMS stamping method.[32]

Cavity-Resonant Spectrum Measurement: A homebuilt confocal microscopy system measures the resonant spectrum of the cavities.[45] The light from a telecom-band wavelength-tunable laser was directed one end of the waveguide through a side objective lens with a numerical aperture (NA) of 0.40 and a working distance of 20 mm, and the cavity-coupled light was detected by an InGaAs photodetector through a top objective lens with an NA of 0.85 and a working distance of 1.48 mm.

PL Measurement: PL measurements were conducted at room temperature in a dry nitrogen atmosphere.[47] A variable wavelength Ti:sapphire laser was used as the continuous-wave light source, with its power controlled via neutral density filters. The laser beam was focused onto the samples with the top objective lens. The PL spectrum was measured through the same objective lens and detected using a liquid-nitrogen-cooled InGaAs diode array attached to a spectrometer. For PL decay curve measurements, a picosecond supercontinuum pulsed laser (30 ps pulse width and 80 MHz repetition rate) was used. After passing the laser through a monochromator to narrow its spectral line width to ≈10 nm, it was directed onto the sample using the top objective lens. The PL from the $MoTe_2$ was collected through the top objective lens and detected with a superconducting single-photon detector. A time-correlated single-photon counting module was used to collect the data.

Switching Measurement: The $MoTe_2$ flake on the cavity was pumped by the picosecond supercontinuum pulsed laser to modulate the cavity mode. The signal light was injected into one end of the waveguide through the side objective lens, and the modulated signal light was detected by a superconducting single-photon detector through the top objective lens and a bandpass filter with a transmission bandwidth of 12 nm.

Supporting Information

Supporting Information is available from the Wiley Online Library or from the author.

Acknowledgements

This work was supported in part by JSPS (KAKENHI JP22K14624, JP22K14625, JP20H02558, JP23H00262) and MEXT (ARIM JP-MXP1223UT1141). N.F. was supported by RIKEN Special Postdoctoral Researcher Program. The FDTD calculations were performed using the HOKUSAI BigWaterfall supercomputer at RIKEN. The authors acknowledge the Advanced Manufacturing Support Team at RIKEN for technical assistance.

Conflict of Interest

The authors declare no conflict of interest.

Author Contributions

D.Y. and Y.K.K. conceived and designed the experiments. D.Y. performed the experiments and analyzed the data. N.F. assisted the materials transfer, and S.F. aided the construction of measurement setup. D.Y. and Y.K.K. wrote the manuscript with inputs from all authors. Y.K.K. supervised the project.

Data Availability Statement

The data that support the findings of this study are available from the corresponding author upon reasonable request.

Keywords

2D materials, nanocavities, optical switching, photonic crystals, silicon photonics

Received: September 19, 2024
Published online:

[1] D. Thomson, A. Zilkie, J. E. Bowers, T. Komljenovic, G. T. Reed, L. Vivien, D. Marris-Morini, E. Cassan, L. Virot, J.-M. Fédéli, J.-M. Hartmann, J. H. Schmid, D.-X. Xu, F. Boeuf, P. O'Brien, G. Z. Mashanovich, M. Nedeljkovic, *J. Opt.* **2016**, *18*, 073003.
[2] W. Bogaerts, L. Chrostowski, *Laser Photon. Rev.* **2018**, *12*, 1700237.
[3] S. Y. Siew, B. Li, F. Gao, H. Y. Zheng, W. Zhang, P. Guo, S. W. Xie, A. Song, B. Dong, L. W. Luo, C. Li, X. Luo, G. Q. Lo, *J. Lightwave Technol.* **2021**, *39*, 4374.
[4] R. Soref, *APL Photonics* **2018**, *3*, 021101.
[5] Z. Chai, X. Hu, F. Wang, X. Niu, J. Xie, Q. Gong, *Adv. Opt. Mater.* **2016**, *5*, 1600665.
[6] T. A. Ibrahim, W. Cao, Y. Kim, J. Li, J. Goldhar, P. T. Ho, C. H. Lee, *IEEE Photon. Technol. Lett.* **2003**, *15*, 36.
[7] V. R. Almeida, C. A. Barrios, R. R. Panepucci, M. Lipson, *Nature* **2004**, *431*, 1081.
[8] T. Tanabe, M. Notomi, S. Mitsugi, A. Shinya, E. Kuramochi, *Appl. Phys. Lett.* **2005**, *87*, 151112.
[9] T. Tanabe, K. Nishiguchi, A. Shinya, E. Kuramochi, H. Inokawa, M. Notomi, K. Yamada, T. Tsuchizawa, T. Watanabe, H. Fukuda, H. Shinojima, S. Itabashi, *Appl. Phys. Lett.* **2007**, *90*, 031115.
[10] X. Hu, P. Jiang, C. Ding, H. Yang, Q. Gong, *Nat. Photonics* **2008**, *2*, 185.
[11] M. Waldow, T. Plötzing, M. Gottheil, M. Först, J. Bolten, T. Wahlbrink, H. Kurz, *Opt. Express* **2008**, *16*, 7693.
[12] C. Husko, A. De Rossi, S. Combrié, Q. V. Tran, F. Raineri, C. W. Wong, *Appl. Phys. Lett.* **2009**, *94*, 021111.
[13] K. Nozaki, T. Tanabe, A. Shinya, S. Matsuo, T. Sato, H. Taniyama, M. Notomi, *Nat. Photonics* **2010**, *4*, 477.
[14] J. S. Pelc, K. Rivoire, S. Vo, C. Santori, D. A. Fattal, R. G. Beausoleil, *Opt. Express* **2014**, *22*, 3797.
[15] G. Dong, W. Deng, J. Hou, L. Chen, X. Zhang, *Opt. Express* **2018**, *26*, 25630.
[16] M. Takiguchi, N. Takemura, K. Tateno, K. Nozaki, S. Sasaki, S. Sergent, E. Kuramochi, T. Wasawo, A. Yokoo, A. Shinya, M. Notomi, *ACS Photonics* **2020**, *7*, 1016.
[17] D. Liang, G. Roelkens, R. Baets, J. E. Bowers, *Materials* **2010**, *3*, 1782.
[18] M. J. R. Heck, J. F. Bauters, M. L. Davenport, J. K. Doylend, S. Jain, G. Kurczveil, S. Srinivasan, Y. Tang, J. E. Bowers, *IEEE J. Sel. Topics Quantum Electron.* **2013**, *19*, 6100117.
[19] G. Roelkens, L. Liu, D. Liang, R. Jones, A. Fang, B. Koch, J. Bowers, *Laser Photon. Rev.* **2010**, *4*, 751.
[20] Z. Wang, A. Abbasi, U. Dave, A. De Groote, S. Kumari, B. Kunert, C. Merckling, M. Pantouvaki, Y. Shi, B. Tian, K. Van Gasse, J. Verbist, R. Wang, W. Xie, J. Zhang, Y. Zhu, J. Bauwelinck, X. Yin, Z. Hens, J. Van Campenhout, B. Kuyken, R. Baets, G. Morthier, D. Van Thourhout, G. Roelkens, *Laser Photon. Rev.* **2017**, *11*, 1700063.
[21] H. Chen, C. Wang, H. Ouyang, Y. Song, T. Jiang, *Nanophotonics* **2020**, *9*, 2107.
[22] J. You, Y. Luo, J. Yang, J. Zhang, K. Yin, K. Wei, X. Zheng, T. Jiang, *Laser Photon. Rev.* **2020**, *14*, 2000239.
[23] Z. Cheng, R. Cao, K. Wei, Y. Yao, X. Liu, J. Kang, J. Dong, Z. Shi, H. Zhang, X. Zhang, *Adv. Sci.* **2021**, *8*, 2003834.
[24] F. Xia, H. Wang, D. Xiao, M. Dubey, A. Ramasubramaniam, *Nat. Photon.* **2014**, *8*, 899.
[25] L. Huang, A. Krasnok, A. Alú, Y. Yu, D. Neshev, A. E. Miroshnichenko, *Rep. Prog. Phys* **2022**, *85*, 046401.
[26] A. Chaves, J. G. Azadani, H. Alsalman, D. R. da Costa, R. Frisenda, A. J. Chaves, S. H. Song, Y. D. Kim, D. He, J. Zhou, A. Castellanos-Gomez, F. M. Peeters, Z. Liu, C. L. Hinkle, S.-H. Oh, P. D. Ye, S. J. Koester, Y. H. Lee, P. Avouris, X. Wang, T. Low, *npj 2D Mater. Appl.* **2020**, *4*, 29.
[27] D. Akinwande, C. Huyghebaert, C.-H. Wang, M. I. Serna, S. Goossens, L.-J. Li, H.-S. P. Wong, F. H. L. Koppens, *Nature* **2019**, *573*, 507.
[28] C. Javerzac-Galy, A. Kumar, R. D. Schilling, N. Piro, S. Khorasani, M. Barbone, I. Goykhman, J. B. Khurgin, A. C. Ferrari, T. J. Kippenberg, *Nano Lett.* **2018**, *18*, 3138.
[29] M. Notomi, E. Kuramochi, H. Taniyama, *Opt. Express* **2008**, *16*, 11095.
[30] M. Eichenfield, R. Camacho, J. Chan, K. J. Vahala, O. Painter, *Nature* **2009**, *459*, 550.
[31] R. Miura, S. Imamura, R. Ohta, A. Ishii, X. Liu, T. Shimada, S. Iwamoto, Y. Arakawa, Y. K. Kato, *Nat. Commun.* **2014**, *5*, 5580.
[32] N. Fang, D. Yamashita, S. Fujii, K. Otsuka, T. Taniguchi, K. Watanabe, K. Nagashio, Y. K. Kato, *Adv. Opt. Mater.* **2022**, *10*, 2200538.
[33] Q. Quan, M. Loncar, *Opt. Express* **2011**, *19*, 18529.
[34] H. Machiya, D. Yamashita, A. Ishii, Y. K. Kato, *Phys. Rev. Res.* **2022**, *4*, L022011.
[35] D. Yamashita, H. Machiya, K. Otsuka, A. Ishii, Y. K. Kato, *APL Photonics* **2021**, *6*.
[36] Z. Chi, H. Chen, Q. Zhao, Y.-X. Weng, *J. Chem. Phys.* **2019**, *151*.
[37] B. Chen, H. Sahin, A. Suslu, L. Ding, M. I. Bertoni, F. M. Peeters, S. Tongay, *ACS Nano* **2015**, *9*, 5326.
[38] M. Fujita, B. Gelloz, N. Koshida, S. Noda, *Appl. Phys. Lett.* **2010**, *97*, 121111.
[39] S. Ahn, G. Kim, P. K. Nayak, S. I. Yoon, H. Lim, H.-J. Shin, H. S. Shin, *ACS Nano* **2016**, *10*, 8973.
[40] Y. Yu, E. Palushani, M. Heuck, N. Kuznetsova, P. T. Kristensen, S. Ek, D. Vukovic, C. Peucheret, L. K. Oxenløwe, S. Combrié, A. de Rossi, K. Yvind, J. Mørk, *Opt. Express* **2013**, *21*, 31047.
[41] Y. Yu, E. Palushani, M. Heuck, D. Vukovic, C. Peucheret, K. Yvind, J. Mork, *Appl. Phys. Lett.* **2014**, *105*, 071112.
[42] P. E. Barclay, K. Srinivasan, O. Painter, *Opt. Express* **2005**, *13*, 801.
[43] M. Notomi, A. Shinya, S. Mitsugi, G. Kira, E. Kuramochi, T. Tanabe, *Opt. Express* **2005**, *13*, 2678.
[44] T. Uesugi, B.-S. Song, T. Asano, S. Noda, *Opt. Express* **2006**, *14*, 377.
[45] D. Yamashita, T. Asano, S. Noda, Y. Takahashi, *Optica* **2018**, *5*, 1256.
[46] C. Ruppert, B. Aslan, T. F. Heinz, *Nano Lett.* **2014**, *14*, 6231.
[47] A. Ishii, M. Yoshida, Y. K. Kato, *Phys. Rev. X* **2019**, *9*, 041048.